STING: a soft-tissue intervention and neurosurgical guide to access deep brain lesions through curved trajectories

L Frasson[1,2], **S Y Ko**[1], **A Turner**[1,2], **T Parittotokkaporn**[2], **J F Vincent**[3], and **F Rodriguez y Baena**[1,2]*
[1]Department of Mechanical Engineering, Imperial College London, London, UK
[2]The Institute of Biomedical Engineering, Imperial College London, London, UK
[3]Department of Mechanical Engineering, University of Bath, Bath, UK

The manuscript was received on 20 May 2009 and was accepted after revision for publication on 17 July 2009.

DOI: 10.1243/09544119JEIM663

Abstract: Current trends in surgical intervention favour a minimally invasive approach, in which complex procedures are performed through very small incisions. Specifically, in neurosurgery there is a need for minimally invasive keyhole access, which conflicts with the lack of manoeuvrability of conventional rigid instruments. In an attempt to address this shortcoming, the current state of progress is reported on a soft-tissue intervention and neurosurgical guide (STING) to access deep brain lesions through curved trajectories. The underlying mechanism of motion, based on the reciprocal movement of interlocked probe segments, is biologically inspired and was designed around the unique features of the ovipositor of certain parasitic wasps. Work to date has focused on probe development, low- and high-level control, and trajectory planning. These aspects are described, together with results on each aspect of the work, including biomimetic microtexturing of the probe surface. Progress is very encouraging and demonstrates that forward motion into soft tissue through a reciprocating mechanism is indeed viable and can be achieved through a suitable combination of microtexturing and microfabrication techniques.

Keywords: medical robotics, biomimetics, wood-boring wasp, needle steering, soft-tissue surgery, steerable probe

1 INTRODUCTION

The brain is one of the most delicate organs in the body: despite the homogeneous appearance of cerebral tissue, brain functions are highly organized in an extremely complex network which controls all physical and cognitive human behaviour. For this reason, surgical interventions into the brain need to be precise, accurate, and safe, and these requirements, coupled with the need to provide surgeons with improved ergonomics and enhanced visualization, dexterity, and haptic feedback, are the focus of current research into computer- and robotic-assisted neurosurgery [**1**]. These efforts can be broadly subdivided into those pertaining to the development of better imaging and modelling methods for the planning of complex brain-related pathologies, and those which focus on the intervention itself: advanced surgical tools for accurate neurosurgery through increasingly smaller incisions.

Advances in both these technologies have, in recent years, enabled surgeons to adopt a minimally invasive approach for a number of procedures, which, until recently, were performed through conventional open-skull surgery. This new set of interventional, diagnostic, and investigative techniques are often grouped together under the term 'keyhole neurosurgery' [**2**], where long thin instruments are used to access different brain regions through a small cylindrical aperture in the skull (usually less than 1 cm in diameter). Tumour

**Corresponding author: Department of Mechanical Engineering, Imperial College London, Exhibition Road, London SW7 2AZ, UK.*
email: f.rodriguez@imperial.ac.uk

biopsies, catheter insertions, deep-brain stimulation (DBS), aspiration and evacuation of deep-brain haematomas, minimal access craniotomies, localized drug delivery, localized chemotherapy and brachytherapy, functional data acquisition, as well as tissue sampling for histological studies, are among the procedures which either can or will be performed in the near future through a minimally invasive approach [**2**–**4**].

These techniques rely heavily on the use of pre-operative imaging (e.g. magnetic resonance imaging (MRI) and positron emission tomography), which enables complex procedures to be planned pre-operatively with accuracy. The location, size, and approach for one or multiple targets can be carefully controlled in relation to adjacent structures in order to minimize risk. Intra-operatively, minimally invasive instrumentation can then be inserted through a keyhole in the skull of the patient, with the aid of a stereotactic frame or of a neuronavigation system (e.g. Brainlab Gmbh. VectorVision^{TM}), which is used to direct the entry point and the required position and orientation of the instrument with respect to the patient position in the operating theatre.

However, while imaging technology and understanding of brain pathology, physiology, and function have improved dramatically in recent years, few technological breakthroughs have affected the intra-operative instrumentation used in minimally invasive neurosurgery on a broad scale. Conventional rigid instruments limit entry paths to follow a straight-line trajectory, which drastically reduces the planning choices that a surgeon is able to make to maximize safety during the insertion process. There have been efforts to improve the safety and accuracy of minimally invasive neurosurgical procedures through the development of 'shared control' systems. A clear example of this trend is Neuroarm, an MRI-compatible image-guided computer-assisted device specifically designed for neurosurgery (microsurgery and biopsy–stereotaxy applications), which has been used to perform the world-first teleoperated tumour removal procedure at Foothills Medical Centre earlier in 2008 [**5**]. Their effectiveness, however, is limited by the predominantly passive nature of their function and by the limitations which are inherent in conventional instruments.

Taking inspiration from nature, a novel soft-tissue steerable probe is currently being developed at Imperial College. It will enable minimally invasive instrumentation to be accurately placed anywhere within the brain by exploiting the unique action of the ovipositor of a wood-boring wasp. By means of a novel smart actuator mechanism, the probe will be able to be steered along curved paths within the body by 'displacing' the tissue in its path (e.g. using a syringe needle). Clearly, this device has the potential to benefit both patients and healthcare providers through better targeting, reduced tissue damage, reduced morbidity, and the potential for developing novel diagnostic tissue sampling and localized therapy procedures, but much work is still needed for this aim to be fulfilled.

In conventional neurosurgery, where optical tracking is used, the tools are rigid and so the handle can be tracked and the location of the tip inferred from the geometry. The availability of small electromagnetic trackers that can be located at the tool tip ensures that the location is obtained directly and thus permits the use of flexible probes.

This paper describes the progress to date on the development of a flexible probe for neurosurgery (a soft-tissue intervention and neurosurgical guide (STING)), which is currently being supported by national funding from the Engineering and Physical Sciences Research Council (EPSRC), as well as a more recent European Union Framework 7 project (EU-FP7), which aims to exploit the findings of this work within a larger integrated project framework. The results to date on probe design and development, low- and high-level control, and pre-operative planning are presented in the following sections.

2 SYSTEM OVERVIEW

EU-FP7 is currently supporting an international project code-named ROBOCAST (robot and sensors integration for computer assisted surgery and therapy [**6**]), which aims to develop a system for robot-assisted, minimally invasive neurosurgery based on the integration of information and communication technologies, scientific methods, and technologies for surgical application, such as minimally invasive burr-hole tumour biopsy, multiple targeting for localized tumour therapy, tissue sampling, liquid microdialysis, multiple-cyst drainage, and electrode placement for DBS.

In the ROBOCAST project, a six-axis serial gross positioning robot (Prosurgics Ltd, UK) is used to support a miniature parallel robot (MAZOR Ltd, Israel) holding a biomimetic soft-tissue steerable probe (Imperial College, UK) to be introduced through a keyhole opening in the skull of the patient; path planning inside and outside the body will be autonomously proposed by the control system by

processing pre-operative diagnostic information (Politecnico di Milano, Italy), while an electromagnetic position sensor, embedded at the tip of the flexible probe, will provide a closed-loop control system with the current position of the probe tip inside the brain (the ROBOCAST system overview is shown in Fig. 1). All robot subsystems will be directed by a high-level controller (University of Karlsruhe, Germany), which will be responsible for the correct and safe operation of all modules (overall system motion planning, collision avoidance, faults monitoring, etc.), to be accessed through a common object request broker architecture (CORBA) interface [**7**]. While a small entry hole in the skull minimizes brain shift (which results from the escape of cerebrospinal fluid from the incision in the *dura*), within the ROBOCAST consortium the use of intra-operative ultrasound technology is planned to enable the real-time monitoring of any brain-shifted features (University of Munich, Germany).

In the context of ROBOCAST, Imperial College's probe will enable minimally invasive instrumentation, exemplified by a localized and multiple-targeting drug delivery system, to reach the target accurately through curved paths within the brain, following minimum-risk trajectories provided by a brain risk atlas, minimizing tissue damage and avoiding buckling, which thus results in better targeting and reduced morbidity.

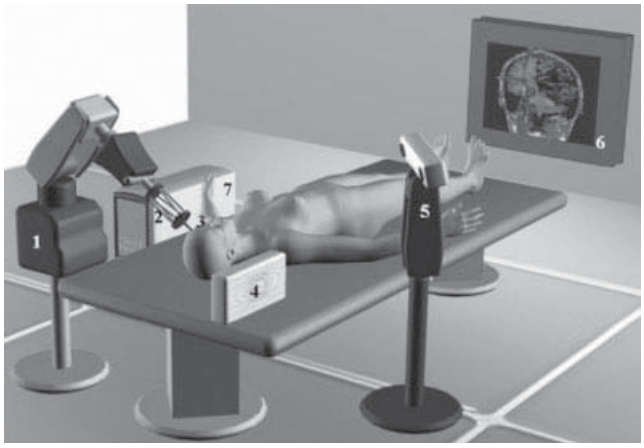

Fig. 1 The ROBOCAST system at a glance. A six-axis serial gross positioning robot 1 is used to support a miniature parallel robot 2 holding the biomimetic steerable probe 3 to be introduced through a keyhole opening in the skull of the patient; an electromagnetic tracking system 4 is used to control position and orientation of the steerable probe tip, while an optical tracking system 5 monitors the robot and patient positions; operative images are visualized on a screen 6 and a central station 7 is in charge of the supervision of the system [**6**]

3 BIOMIMETIC FOUNDATIONS

Nature has inspired amongst the most diverse and demanding engineering tasks and many successful examples can be found in the area of biomedical engineering: Menciassi *et al.* [**8**] developed a microrobot for semiautonomous colonoscopy which replicates the locomotion principle of earthworms; the design and the mechanics of a mosquito's proboscis have also inspired different research groups for the development of more effective and less painful microneedles for skin blood sampling [**9**–**11**].

The strategy developed by different kinds of ovipositing wasps which penetrate a variety of tissues (e.g. wood, leaves, and host larvae) in order to lay eggs is the source of inspiration for the novel flexible and steerable probe for neurosurgery described here. Ovipositing wasps, whether parasitic (egg-laying in host larvae) or non-parasitic (eggs are inserted into some substrate, such as wood), carefully choose the location for their eggs before steering the ovipositor towards a desired target. The typical structure of the ovipositor is shown in Fig. 2: a single upper valve (*valvus*), together with a pair of lower valves forms a lumen through which eggs can pass; the upper valve is interlocked with both the lower valves by means of a 'T-section' longitudinal ridge (*rachis*), which runs within a corresponding groove (*aulax*) on the lower valve, thus forming the *olistheter* mechanism. The ovipositor can be very long and thin (0.1–0.2 mm in diameter and up to 50 mm long), is highly flexible (0.5 mm minimum bending radius) and, despite

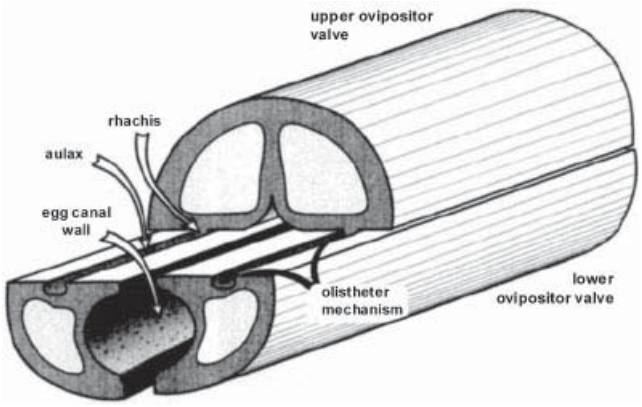

Fig. 2 Diagrammatic representation of the oblique view of a transversely cut ovipositor with lower valves protruding [**12**]

being devoid of intrinsic musculature, can penetrate tissues as rigid as wood, while avoiding buckling. Two main factors underlying this behaviour have been proposed: the 'toothed' surface of the ovipositor tip and the insertion mechanism, which is based on reciprocal motion. Figure 3 and Fig. 4 illustrate how different surface topographies evolved for the penetration of different tissues: *Sirex noctilio* bores into wood to lay eggs, where some teeth are used to provide purchase during the insertion, while others are used to cut the tissue; *Orussus abietinus* penetrates a host larva more softly but firmly, without endangering the host itself. These anisotropic surfaces are coupled with the unique reciprocal motion of the ovipositor to achieve tissue penetration with minimum axial push, thus avoiding buckling; the pull on one of the valves provides stabilization along the length of the ovipositor so that the other valve can be pushed with an equal and opposite force, to produce a net force near zero; the reciprocating motion of the two valves drives the ovipositor's forward motion, as one valve is pushed deeper into the tissue stabilized by the tension generated in the other valve. Since there is virtually no net force in the ovipositor assembly, there are no stability problems and there is no theoretical limit on its length [**12**–**14**].

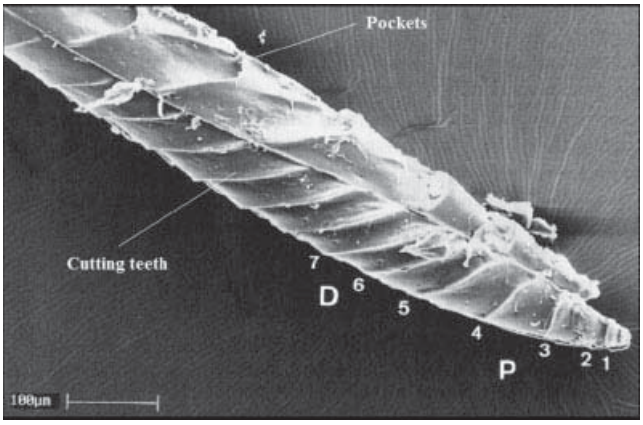

Fig. 3 The tip of the ovipositor of *Sirex noctilio*. Teeth 1 to 4 (P) point proximally and are 'pull teeth'; teeth 6 and 7 and higher (D) point distally and are 'push teeth' [**13**]

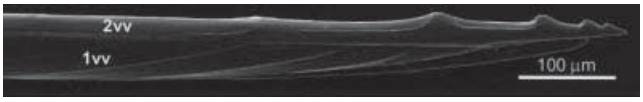

Fig. 4 *Orussus abietinus* ovipositor tip [**14**]: 1vv, first valvula (lower valve); 2vv, second valvula (upper valve)

The ovipositors have no intrinsic musculature and all their movements have to result from the actions of muscles inside the abdomen, but in many species the tip can be guided independently, allowing it to play a more active part in host localization; some wasps can even locate particular structures within the prey, while others need to lay eggs in a number of adjacent locations. The ability to bend the ovipositor is thus a considerable advantage which enables the wasp to penetrate the substrate at a different location without the need to withdraw the tip completely. Thus, ovipositing wasps are also a source of inspiration for the steering mechanism of a multi-part probe for brain penetration, where no 'active components' are located inside the probe itself; the bending mechanism can rely upon the tissue–probe interaction and the interaction between the different parts of the probe [**15**, **16**].

4 MATERIALS AND METHODS

The block diagram in Fig. 5 shows the architecture of the system; pre-operative diagnostic images (MRI images showing the location of the deep-brain target), together with the physical constraints imposed by the flexible probe (minimum radius of curvature) will be processed by the 'high-level controller', which supplies the 'path of minimum risk' for a specific intervention based on digital brain segmentation, a risk grading of brain areas, and a suitable path planning algorithm; on the basis of this minimum-risk trajectory, the 'low-level controller' generates the motion signals required to actuate the flexible probe. An electromagnetic position sensor, embedded at the tip of the flexible probe, will provide the position feedback to control probe motion, which in turn will enable path following. An overview of the work performed to date on the three main modules constituting the system will follow: hardware development, low-level control and high-level control.

4.1 Flexible probe development

Figure 6 illustrates the testing set-up which was proposed to prove the concept of 'forward motion through a reciprocating mechanism', as experienced by ovipositing wasps; by reciprocally actuating the two valves comprising the flexible ovipositor, the wasp can penetrate the tissue while exerting minimum axial force from the back. A simplified equation describing this behaviour is proposed

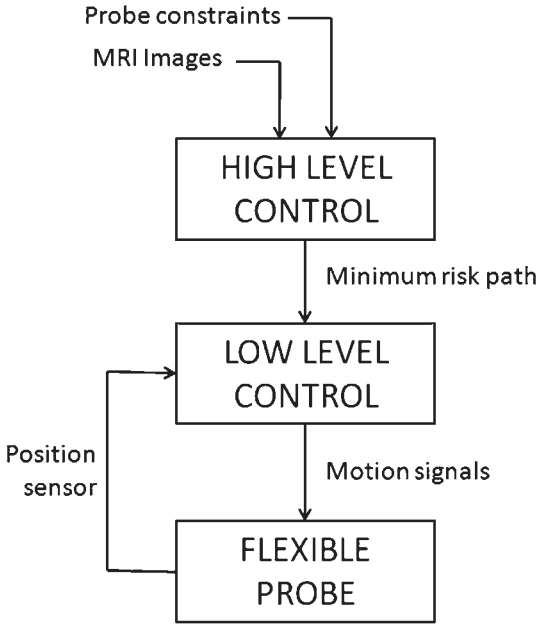

Fig. 5 Block diagram of the system architecture. The high-level controller takes into consideration pre-operative images (e.g. MRI and computed tomography (CT)) and probe constraints (e.g. maximum radius of curvature) to define a minimum risk path inside the brain, which will then be used by the low-level controller to generate appropriate motion signals to drive the probe towards the target. A position sensor (e.g. electromagnetic tracker) will provide tip position feedback

according to

$$F_c + F_i < F_d < F_e \tag{1}$$

where F_c is the force required at the tip of the probe to cut and displace the tissue, F_i is the force caused by the probe surface sliding against the tissue which is compressing the probe shaft during insertion, F_e is the force caused by the probe surface grasping the tissue when attempting to remove the probe from the tissue, and F_d is the force used to push the moving half of the probe inwards.

Two main steps have been identified in order to prove the concept of reciprocal motion: probe–tissue interaction characterization and forward motion through a reciprocating mechanism. This early work has been described in detail by Frasson *et al.* [**17**] and Parittotokkaporn *et al.* [**18**] respectively, but a summary is provided here for completeness.

The first step required to prove the concept of reciprocal motion was to identify a suitable anisotropic surface texture for the probe, which satisfies equation (1), without causing tissue damage during the insertion and the extraction of the probe itself into soft tissue. For this test, rigid needles with toothed surfaces were manufactured (Fig. 7) and then tested into pig brain by measuring the force required to insert and extract the needle. In this proof-of-concept experiment, two main tooth geometries were chosen (triangular teeth and fin-like

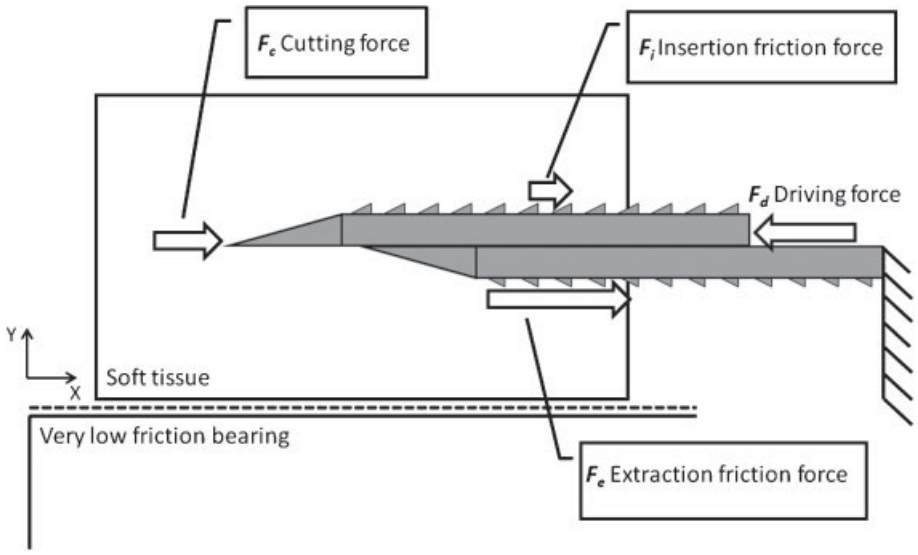

Fig. 6 Diagrammatic representation of the forces involved during one step of the reciprocal motion; the lower valve is stationary, while the upper valve is pushed inside the tissue. The extraction frictional force exerted by the stationary valve avoids the tissue moving to the left, together with the upper moving part, on the very-low-friction bearing

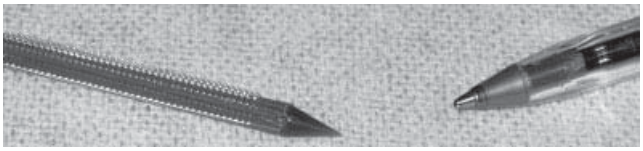

Fig. 7 Assembled needle with fin-like 500 μm teeth

teeth), with tooth sizes ranging from 10 μm to 500 μm (Fig. 8). The results of this set of experiments demonstrated how very small surface topographies (down to 10 μm) affect the forces experienced in the two directions of motion, facilitating the insertion of the rigid probe and increasing the gripping force during needle extraction. However, it was shown that, considering the peak forces experienced, insertion still requires greater force than extraction, owing to the relatively high force experienced by the needle tip during first insertion (i.e. F_c).

The second step was then to actuate the two parts of a simplified probe assembly, which included a suitable anisotropic surface at the probe–tissue interface; if the probe could be inserted into a tissue sample positioned on a very-low-friction bearing (to minimize all other external forces) without the need for an overall axial push, the concept would be validated. The rig set-up employed for this experiment is shown in Fig. 9. Two textured samples (with geometrical and dimensional tooth features identical with those used in the first step) are reciprocated on to the surface of two synthetic soft-tissue samples mimicking brain consistency (0.5 wt % agar gel and 60 wt % gelatin [**19**, **20**]) positioned on a frictionless air bearing surface. This simplified set-up was chosen to isolate the sliding–gripping behaviour of an anisotropic surface when moved in two different directions, in the absence of any cutting forces which would be experienced by the tip of the probe during insertion. The results, published in reference [**18**], demonstrated that soft-tissue traversal with 'zero net force' is viable, but it is highly dependent on the material tested; a mix of plastic and cutting behaviour is required to provide sufficient grip between the small teeth of the sample and the tissue itself. For instance, the hyperelastic characteristics of gelatin prevent the teeth from indenting and gripping the tissue, resulting in the absence of

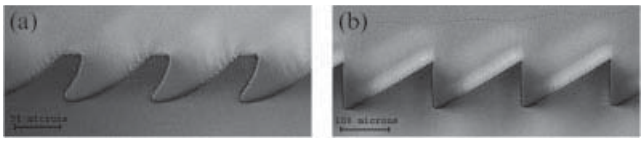

Fig. 8 Optical microscope view of (a) the 50 μm fin-like teeth and (b) the 100 μm triangular teeth

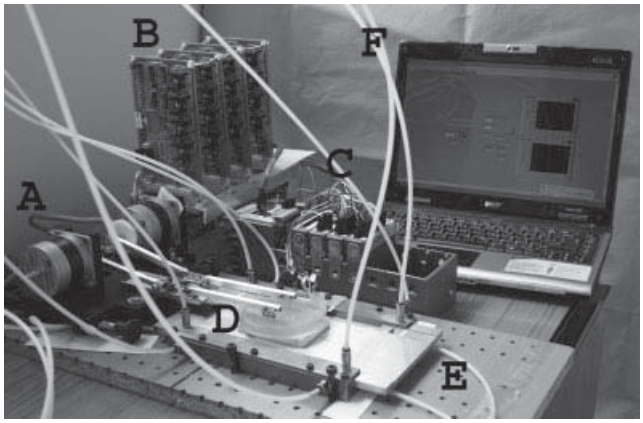

Fig. 9 Experimental rig set-up including two stepper motors A and corresponding electronics B, a CompactRIO controller C, reciprocating mechanism D, low-friction air bearing with optical encoder E, and control laptop running LabView 8.5 F

forward motion during the reciprocating experiment.

On the basis of these early experiments, which justify current work on the development of a biologically inspired flexible probe for neurosurgery, the key assumption of anisotropic surface texturing as an aid to forward motion by means of a reciprocating mechanism was demonstrated. A preliminary flexible probe made of two interlocking halves is currently in the early stages of manufacture and is shown in Fig. 10. The probe is made via rapid prototyping in a soft rubber-like material with high elasticity (Tango Black^{TM}, Objet; tensile strength, 2 MPa; Shore A hardness, 61; elongation at break, 47.7 per cent), has an outer diameter of 4.4 mm, and is highly flexible. A first set of tests is planned on this prototype to ascertain the final geometry and size of the probe and to investigate the steering mechanism, which represents an ongoing research challenge. A final prototype of the segmented probe, which is due

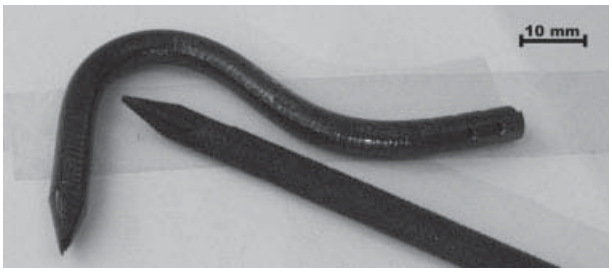

Fig. 10 Flexible probe prototypes: each probe is 4.4 mm in diameter, is made of two interlocked halves, and shows a very high degree of flexibility

to be employed in laboratory trials starting in December 2010, will be manufactured in silicone, using an extrusion process for better mechanical performance and tighter tolerances on the geometrical features. This final set of trials will focus on the prototype's performance and trajectory following capabilities on a plane, while miniaturization of the probe's outer diameter (down to a size similar to current endoscopes and ventriculostomy needles [**21**]) will be addressed in the longer term. Finite element simulations for the interlock section geometry and the material properties optimization are also currently under way [**22**].

4.2 Curvature-based control of a steerable probe

Recent studies have shown that, as a flexible needle with a bevel tip is pushed through soft tissue, the asymmetry of the tip itself causes the needle to bend to follow a curved trajectory; Webster *et al.* [**23**] proposed that a properly designed needle can be steered through tissue to reach a specified target. Their modelling results show that the bevelled-tip flexible needle has a motion with two degrees of freedom. The first degree of freedom corresponds to the insertion of the needle and produces a circular trajectory as it travels through the tissue in the longitudinal direction. The second corresponds to pure rotation of the needle along its longitudinal axis. Following these results, Minhas *et al.* [**24**] were able to develop a control strategy to alter the trajectory of the bevel tip during insertion; proportional control of the curvature of the trajectory was achieved via duty-cycled spinning of the needle itself, where the approach angle of the needle can be controlled through a cyclical rotation along the longitudinal axis. More recently, Kallem and Cowan [**25**] proposed image guidance of the flexible tip as a means to compensate for errors during path following.

The main shortcoming of the bevelled-tip approach to needle steering pertains to limitations in the cross-sectional diameter of the needle, which is inherent to the steering mechanism itself. Since trajectory control is achieved through duty cycling, the material which the needle is made of needs to be sufficiently stiff to enable the transmission of a torsional force along the entire length of the needle (which explains the choice of a nitinol stranded wire), while the diameter should be small enough for the needle to be flexible and thus able to bend (currently 0.28 mm [**24**]). Given the contrasting requirements of a stiff material coupled with the need for a highly flexible needle, such limitation on the maximum outer diameter cannot be exceeded under any circumstance.

In contrast, the biomimetic design proposed here has no such limitation on diameter size, since motion is achieved through the reciprocating motion of interlocked halves, which enables the needle to be 'pulled from the front' as opposed to be pushed from the back. As a result, the design provides no theoretical constraint on the probe diameter or maximum length, and thus its ability to bend, which is seen to be a unique advantage of this design over alternative solutions.

A different approach is proposed by Glozman and Shoham [**26**], where a standard rigid needle is steered along a curved trajectory inside soft tissue (turkey breast muscle). In order to avoid obstacles, the needle (a 22-gauge spinal needle; outer diameter, 0.711 mm) is bent by applying a momentum at its base and the insertion trajectory is planned by modelling tissue and needle interaction and deformation. However, since the targeting performance relies highly upon tissue stiffness and resistance, a similar approach on a tissue as soft as brain is not applicable and may result in severe tissue damage.

While a suitable steering mechanism for STING is currently under development, a curvature-based control of the steerable probe has been developed and is described in the following sections. It is assumed that both the curved trajectory and the motion of the needle lie on one plane and that the probe itself is steerable, which means that the approach angle can be changed. Finally, it is assumed that the probe tip position and orientation are known, since an electromagnetic tracking sensor, embedded in the tip of the probe, is expected to be available in the final embodiment of the prototype.

4.2.1 Kinematic model of probe motion

Assuming that the probe can be steered, a curved trajectory can be described in terms of a variable radius R or a variable curvature $\rho = 1/R$, which corresponds to the orientation of the tip with respect to a global coordinate system. In order to describe the kinematics of the probe, the standard non-holonomic model for a single wheel was adopted [**27**]. It was shown that this model, the so-called 'unicycle model', can be applied to express the behaviour of a bevelled-tip probe by Webster *et al.* [**23**]; according to their model, the probe's trajectory follows a circular motion with a fixed radius as it is

inserted along the longitudinal direction while keeping its orientation along its longitudinal axis. In the model described here, the rotational radius is considered to be variable so that the probe can trace the desired trajectory by changing its curvature ρ.

The discrete implementation of the unicycle model is described by

$$ {}^{w}\mathbf{T}_t(k+1) = {}^{w}\mathbf{T}_t(k)\, e^{u_i \hat{\mathbf{V}}_i \Delta t} \tag{2} $$

where ${}^{w}\mathbf{T}_t$ is the homogeneous matrix given by

$$ {}^{w}\mathbf{T}_t = \begin{bmatrix} {}^{w}\mathbf{R}_t & {}^{w}\boldsymbol{p}_t \\ \boldsymbol{0}^T & 1 \end{bmatrix} \in \mathrm{SE}(3) \tag{3} $$

with the rotational matrix given by ${}^{w}\mathbf{R}_t \in \mathrm{SO}(3)$, and the position of the probe tip in the world coordinate system given by ${}^{w}\boldsymbol{p}_t \in \Re^3$. $\hat{\mathbf{V}}_i$, which is given by

$$ \hat{\mathbf{V}}_i = \begin{bmatrix} 0 & -\rho & 0 & 1 \\ \rho & 0 & 0 & 0 \\ 0 & 0 & 0 & 0 \\ 0 & 0 & 0 & 0 \end{bmatrix} \tag{4} $$

indicates the velocity of the probe tip during insertion. Δt, u_i, and ρ indicate the sampling time of the discrete controller, the insertion velocity, and the curvature of the trajectory respectively. In this definition, the longitudinal direction of the probe and the normal vector of the plane are defined in the x and z directions of the local tip coordinate system respectively. In contrast with reference [**23**], the ability to change the curvature of the motion is assumed here, which enables the development of a closed-loop trajectory control strategy, where the sensory information from the probe tip is used to measure (and correct) the path-following error.

4.2.2 *Curvature control of the probe*

The tracking error of a probe following a curved trajectory can be described in terms of the following:

(a) a 'normal' component (the position error), which corresponds to the distance between the probe tip and its closest point on the path;
(b) an 'approach' component (the slope error), which corresponds to the angular difference between the probe's current approach and the path's tangent vector centred at the closest point.

Thus, to achieve curvature control, a similar concept to conventional proportional–derivative (PD) control is employed; the proportional term corresponds to tip position control, while the derivative term corresponds to slope control. As shown in Fig. 11, the three-dimensional (3D) instantaneous position of the probe tip is $\boldsymbol{P}_t \in \Re^3$, with an approach vector $\boldsymbol{s}_t \in \Re^3$ ($|\boldsymbol{s}_t| = 1$), a curvature of $\rho_t \in \Re^1$, and an insertion velocity $u_i \in \Re^1$.

In order to compute the position and slope errors in discrete steps, the desired position of the probe tip in the following time step needs to be defined with respect to the current position. The desired position $\boldsymbol{P}_{\mathrm{des},\, t+\Delta t}$, which describes the desired position of the tip at time $t+\Delta t$, is defined as the closest point of the position $\boldsymbol{P}_{t+\Delta t}$ of the probe tip on the predefined desired trajectory, as described by

$$ \boldsymbol{P}_{\mathrm{des},\, t} = f_{\mathrm{closest}}(\boldsymbol{P}_t, \mathrm{desired\_trajectory}) \tag{5} $$

$$ \boldsymbol{P}_{\mathrm{des},\, t+\Delta t} = f_{\mathrm{closest}}(\boldsymbol{P}_{t+\Delta t}, \mathrm{desired\_trajectory}) \tag{6} $$

where f_{closest} denotes a closest-point search of the trajectory. The curvature controller then uses the

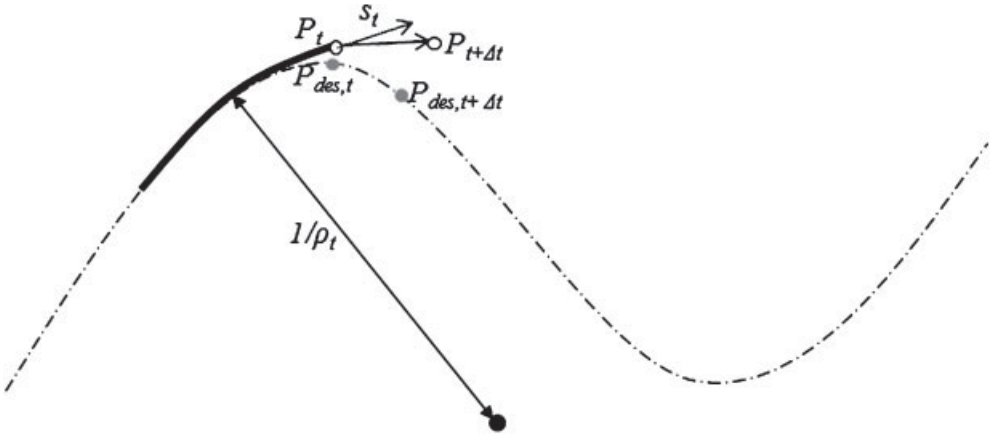

Fig. 11 Probe (thick solid curve) following the predefined trajectory (dot-dashed curve)

estimated position $\boldsymbol{P}_{t+\Delta t}$ to obtain the position error instead of the current position $\boldsymbol{P}_t$, and the next position is estimated using

$$\boldsymbol{P}_{t+\Delta t} = P_t + u_i s_t \, \Delta t \tag{7}$$

where u_i and Δt denote the insertion speed and the sampling time respectively.

The position and slope errors are defined as

$$\varepsilon_{\text{pos}} = \text{sgn}\left[\left(\overline{\boldsymbol{P}_t\boldsymbol{P}_{t+\Delta t}} \times \overline{\boldsymbol{P}_t\boldsymbol{P}_{\text{des},\,t+\Delta t}}\right)\cdot \boldsymbol{e}_{\text{n}}\right]\left|\overline{\boldsymbol{P}_{\text{des},\,t+\Delta t}\boldsymbol{P}_{t+\Delta t}}\right| \tag{8}$$

$$\varepsilon_{\text{slope}} = \frac{\left(\overline{\boldsymbol{P}_t\boldsymbol{P}_{t+\Delta t}} \times \overline{\boldsymbol{P}_{\text{des},\,t}\boldsymbol{P}_{\text{des},\,t+\Delta t}}\right)\cdot \boldsymbol{e}_{\text{n}}}{\left|\overline{\boldsymbol{P}_t\boldsymbol{P}_{t+\Delta t}}\right|\left|\overline{\boldsymbol{P}_{\text{des},\,t}\boldsymbol{P}_{\text{des},\,t+\Delta t}}\right|} \tag{9}$$

respectively, where $\boldsymbol{e}_n$ denotes the normal vector of the plane on which the trajectory lies. The update rule for the desired curvature ρ_{des} is defined in terms of

$$\dot{\rho} = k_{\text{p}}\varepsilon_{\text{pos}} + k_{\text{d}}\varepsilon_{\text{slope}} \tag{10}$$

$$\rho_{\text{des},\,t+\Delta t} = \rho_{\text{des},\,t} + \dot{\rho}\,\Delta t \tag{11}$$

i.e. a similar approach to standard PD control. Figure 12 shows the results of a simple simulation where the kinematic model and the curvature controller described here were preliminarily tested with and without synthetic external disturbances. In this simulation, Gaussian sensor noise with 1 mm/5° standard deviation and Gaussian curvature noise with a standard deviation equal to 10 per cent of the maximum curvature of the probe were chosen. The maximum curvature was set to 0.04 mm^{-1}, which corresponds to a minimum radius of curvature R of 25 mm, as per specification of the biomimetic probe. Figures 12(a), (b), and (c) show the tracking performance, the variation in the curvature ρ, and the position error respectively, when simulated without any sensor noise or low-level control error. Here, the low-level control error indicates the error which is generated by inaccuracies during the control of the actuators driving the probe segments (the characteristics of this noise are equal to those used to simulate sensor noise). Conversely, Figs 12(d), (e), and (f)

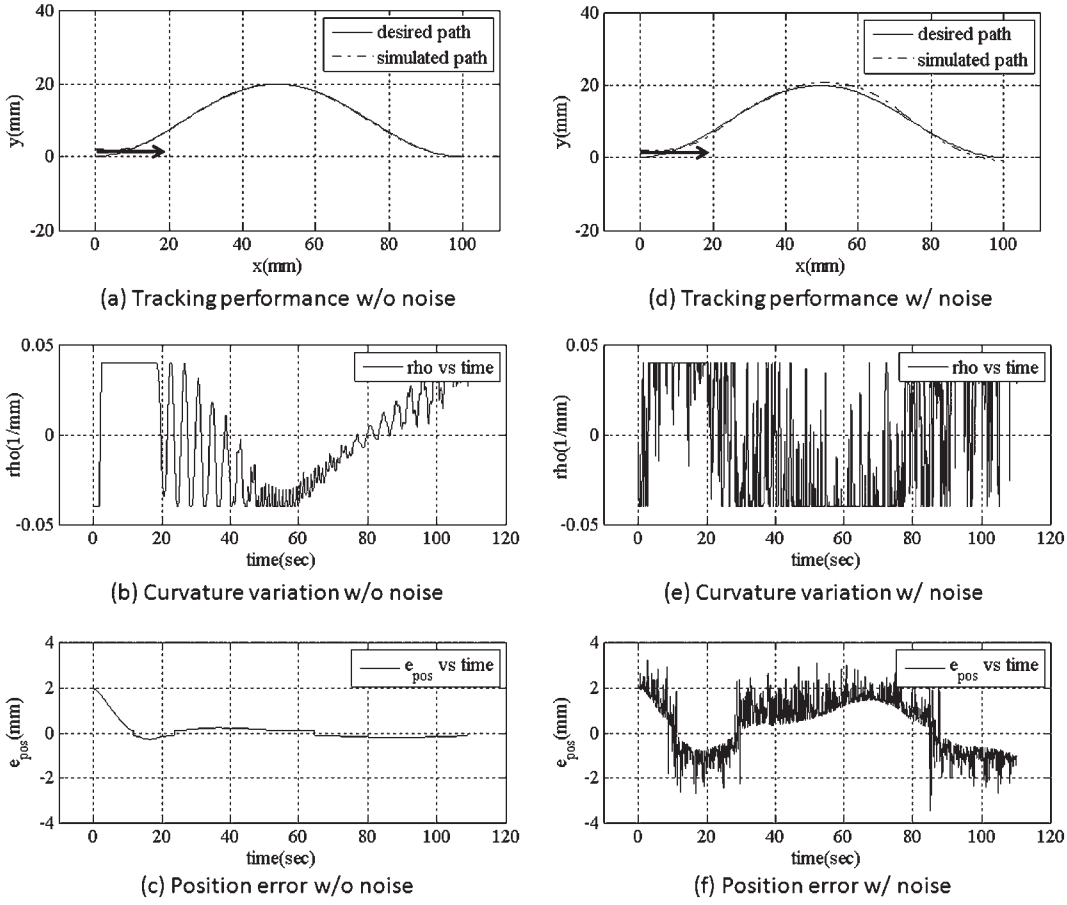

Fig. 12 Tracking performances of the curvature control

illustrate the tracking performance of the controller in the presence of synthetic disturbances (i.e. sensor noise and the low-level control error). The arrows in Figs 12(a) and (d) denote the insertion position, which is set to (0 mm, 2 mm, 0 mm). This simulation shows that the curvature-based control can make the probe follow the predefined trajectory smoothly. Specifically, the maximum position error without any synthetic disturbances was less than 0.3 mm. In the case of disturbances, however, the error increased to about 2 mm, but it will be possible to reduce this value by developing a suitable noise model. In order to guarantee that the probe will not intersect 'high-risk' areas, this error will be accounted for by allowing for a safety margin during path planning. As a point of note, the 'ripples' which can be observed in Figs 12(b) and (e) mainly originate from the closest-point search algorithm, since it was implemented for a discrete trajectory and there exists a small discontinuity of the slope at both sides of the closest point.

4.3 Risk-based trajectory planning

Because of the steerable nature of STING, an infinite number of potentially identical trajectories can be found which intersect a surgeon's chosen entry point and target. It thus becomes necessary to develop means by which desirable trajectories can be found; many route-finding methods generate paths in which, for instance, a robot does not collide with obstacles in its world (e.g. a robot seeking to exit a maze should not collide with walls). This essentially means that the world is divided into mutually exclusive partitions; i.e. areas where the robot *can* go, and areas where it *cannot*.

In the present problem, although there are some obstacles that must be avoided (such as vasculature, neural tracts, and other critical brain structures), the selection of route is not always as clear cut; it may be in some sense preferable to navigate through tissue A than tissue B, but it may still be necessary to penetrate into tissue B in order to reach the desired location. In such a case, a route must be chosen which minimizes risk to the patient.

This problem has been approached using the fast marching method, described by Sethian [**28**], which is a method for solving the Eikonal equation $|\nabla T| = r$; in the present problem, r is the risk associated with the probe occupying a particular spatial location; T is then the minimum integrated risk to reach that location from some start position, where T is defined as zero. The values of r at each spatial location are known in advance; they are based on a risk atlas which will be described shortly. The route to any other point back to the start point can be found by gradient descent. Because of the way that T is calculated, this route is the minimum-risk path between the two points.

As yet, nothing has been said about the kinematic constraints on the route of the probe; the finite minimum radius of curvature of the probe must be taken into account. This can be straightforwardly incorporated into the fast marching method by altering the risk values at each spatial location in the brain, according to an expression for the minimum radius of curvature from Petres *et al.* [**29**]: $R \geqslant \inf T / \sup \|\nabla T\|$. Petres *et al.* stated that the minimum radius of curvature can be increased either by adding an offset to T in order to increase the numerator, or by smoothing T in order to decrease the denominator. The first option is not desirable; the route would tend to travel further through regions of higher risk, since the relative difference between two regions has been reduced.

As such, the kinematic constraint is added by smoothing the risk values, but it is critical that the smoothed risk associated with a particular location is never smaller than the unsmoothed risk. It is thus not acceptable to use straightforward Gaussian blurring, for instance, because this will decrease the apparent risk of traversing high-risk regions. As such, a custom smoothing which guarantees that risk does not decrease has been developed (Fig. 13).

In order to apply a risk-based trajectory-planning algorithm to brain surgery, the principal brain structures need to be labelled and categorized according to the perceived risk associated with the probe intersecting each structure. As a proof-of-concept implementation, two experienced neurosurgeons were asked to rank different brain structures according to risk, then a risk value was defined for each structure to reflect the ranking. A previously

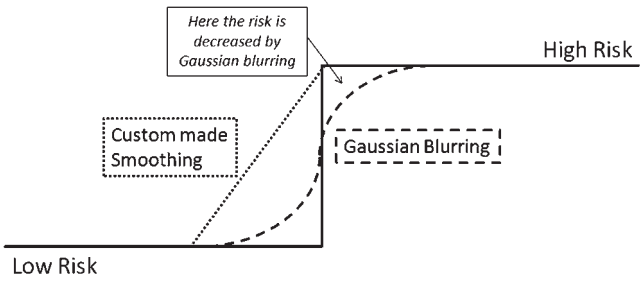

Fig. 13 The custom-made smoothing, compared with Gaussian blurring, which prevents the algorithm from associating with a high-risk area, thereby giving smaller values of risk

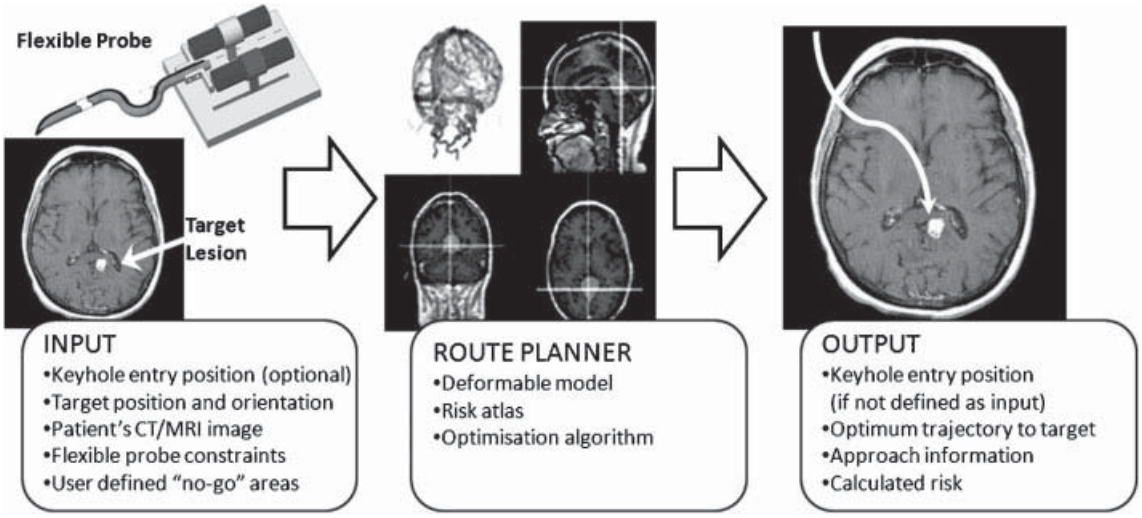

Fig. 14 Route planner for the brain

segmented high-resolution MRI scan of the human brain, separated into 83 anatomical regions, was used for this purpose [**30**]. A software application was also developed to generate two-dimensional (2D) (i.e. planar) routes through the brain, according to the risk value identified for each structure (Fig. 14). Inputs to the software are the desired entry and target points, the minimum radius of curvature (which is a function of the kinematic constraints of the probe) and, optionally, user-defined 'no-go' areas, which can be included in the image slice to account for set-up- or patient-specific constraints (e.g. patient-specific areas of increased danger). The output is a viable trajectory that will intersect the target at minimum risk (i.e. by traversing areas with a reduced risk factor and avoiding areas of high risk).

Figure 15 illustrates the graphical output of one run of the simulation; a coronal section of the brain is shown, where some of the brain regions are labelled and classified according to the risk classification proposed by the experienced neurosurgeons. In this picture, the greyscale value of each region corresponds to a risk classification, where 'white' reflects 'extreme danger'. Here, the globus pallidus is

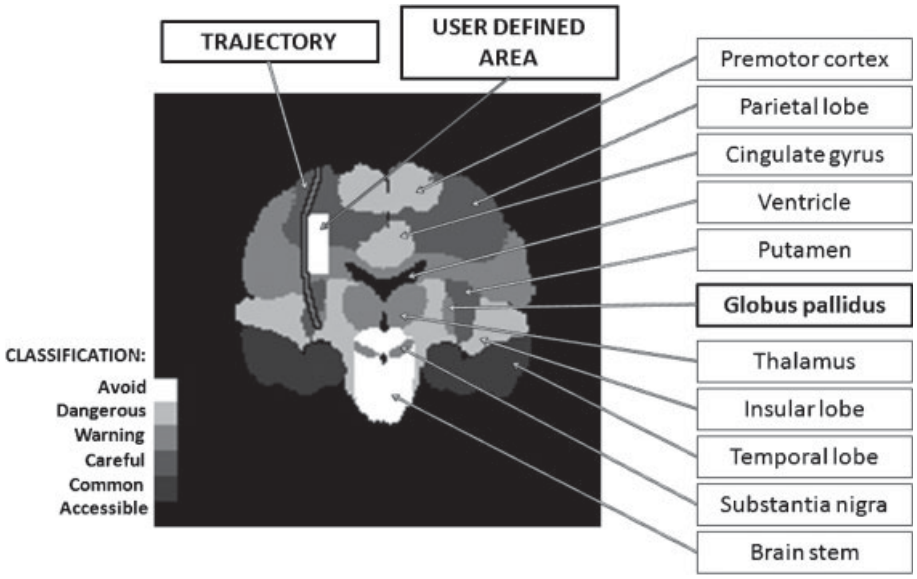

Fig. 15 The route planner for the brain. A coronal section of the brain is labelled and each area classified according to the risk classification shown on the left; the white rectangle represents a user-defined 'avoid area' manually added on the coronal view; the optimum trajectory between the surface of the parietal lobe (entry point) and the globus pallidus (target point) is displayed

chosen as the target point, while a suitable entry point was chosen on the surface of the parietal lobe (DBS electrode placement for people affected by dystonia is generally performed via electrode insertion, through the parietal lobe and putamen, to the globus pallidus). A hypothetical user-defined 'no-go' area (white rectangle) was also included in Fig. 15 for illustration purposes; the optimum trajectory is thus calculated and displayed on the coronal view.

In this 2D proof-of-concept example, the 'no-go' area only serves as a simple geometrical constraint to identify a region which is off-limits on pre-operative image data. Clearly, such a simplified approach would not be suitable for 3D path planning, for which a more complex software interface and better planning tools would need to be developed. On the basis of these successful preliminary proof-of-concept results, however, the concept of a 'route planner for the brain' is currently being extended within the context of the ROBOCAST project (see section 2), where path planning both inside and outside the body is being developed in collaboration with the Politecnico di Milano, Italy. This ongoing work aims to explore risk-based trajectory planning in full three dimensions and will rely upon a segmented brain atlas, a complex risk-based decision tree and image fusion between different modalities (MRI, CT, and magnetic resonance angiography), which are to be implemented within the framework of an open source image library called 3D Slicer [**31**].

5 CONCLUSIONS AND FUTURE DEVELOPMENTS

As many conventional surgical instruments fail to meet the increasing requirements imposed by minimally invasive surgical approaches (e.g. keyhole neurosurgery), research into new advanced tools becomes necessary. This paper outlines the current state of progress on the development of STING, which is used to access deep-brain lesions through curved trajectories. Work to date has focused on probe development, low- and high-level control, and trajectory planning. The biological inspiration of ovipositing wasps provided the basis for the design and development of a multi-part probe which, through a focused set of preliminary experiments, was shown to work as per the original hypothesis; forward motion into soft tissue through a reciprocating mechanism is indeed viable and can be achieved through a suitable combination of microtexturing and microfabrication techniques. While work on a steerable tip, which will enable the probe to traverse soft tissues through curvilinear trajectories, is still under way, these encouraging results justify our continued research effort in this respect.

A suitable control strategy to drive the probe along planar trajectories was also described. A simple curvature-based control algorithm was proposed and typical tracking performances were illustrated via simulation and in the presence of synthetic Gaussian noise to replicate positional sensor error and low-level control error. Simulated results show that the control algorithm provides smooth trajectory-following capabilities even when sensor noise is added to the simulation, and that its implementation is straightforward. As the design of the probe is finalized and a suitable steering mechanism is developed, the capabilities of the controller will be extended to include the mapping of smooth forward motion to cyclical actuator commands, which are needed by the reciprocating mechanism.

Given the steerable nature of STING, an algorithm for safe trajectory planning inside the brain, which takes into account the risk of accessing certain brain areas, was also proposed: a 'route planner' for minimally invasive neurosurgery, where the optimum path between any entry and target point is calculated on the basis of 'minimum risk'. In a proof-of-concept implementation, areas from the presegmented image of a human brain were labelled and ranked according to the severity of dysfunctions related to the potential local damage of such areas. A modified fast marching method was then implemented to calculate the minimum-risk path between two points on a 2D brain slice; to account for kinematic constraints imposed by the probe (e.g. maximum radius of curvature) a custom smoothing of the risk values was also defined. This work provided the motivation for an advanced planning workstation, which is now a topic of research in the ROBOCAST project.

While the progress to date on these aspects of development has been encouraging, a number of important milestones still lie ahead. A flexible probe prototype, suitable for *in-vitro* cadaveric experimentation, needs to be finalized; a suitable steering mechanism needs to be developed and work is currently under way in this respect; the curvature-based controller is to include a mathematical model of the probe actuation strategy, which is then to be tested with a real prototype and live positional information; automatic and user-friendly software for the risk-based trajectory planner needs to be developed in collaboration with partners of the ROBOCAST project (Politecnico di Milano). Within ROBOCAST, which aims to develop a complete

robotic platform for minimally invasive neurosurgery, the integration of a six-axis serial gross positioning robot, a miniature parallel robot and STING, where all robot subsystems are directed by a high-level controller responsible for the correct and safe operation of all modules, is planned for 2010.

ACKNOWLEDGEMENTS

The authors would like to thank the sponsoring bodies EPSRC, Science and Technology Facilities Council, and EU-FP7. The authors would also like to thank Professor Daniel Rueckert for providing the segmented MRI scan of a human brain.

REFERENCES

1 **McBeth, P. B., Louw, D. F., Rizun, P. R.,** and **Sutherland, G. R.** Robotics in neurosurgery. *Am. J. Surg.*, 2004, **188**, 68–75.

2 **Perneczky, A., Müller-Forell, W., van Lindert, E.,** and **Fries, G.** *Keyhole concept in neurosurgery: with endoscope-assisted microsurgery and case studies*, 1999 (Thieme, New York).

3 **Suyama, D., Ito, K., Tanii, M., Furuichi, S., Yoshizawa, T.,** and **Yamagiwa, O.** Neuroendoscopic surgery for intracerebral hematomas using a transparent sheath – technique and results of putaminal, thalamic, and lobar hemorrhages. In *Developments in neuroscience*, Proceedings of the Third International Mt Bandai Symposium for Neuroscience and the Fourth Pan–Pacific Neurosurgery Congress, International Congress Series, Vol. 1259, 2004, pp. 279–286 (Elsevier, Amsterdam).

4 **Badie, B.** Endoscopic and minimally invasive microsurgical approaches for treating brain tumor patients. *J. Neuro-oncol.*, 2004, **69**, 209–219.

5 neuroArm, 2009, available from http://www.neuroarm.org/.

6 Robocast, 2008, available from http://www.robocast.eu.

7 Real-time CORBA with TAO™ (the ACE ORB), 2007, available from http://www.cs.wustl.edu/~schmidt/TAO.html.

8 **Menciassi, A., Gorini, S., Pernorio, G.,** and **Dario, P.** A SMA actuated artificial earthworm. In Proceedings of the IEEE International Conference on *Robotics and Automation*, 2004, Vol. 4, pp. 3282–3287 (IEEE, New York).

9 **Aoyagi, S., Izumi, H.,** and **Fukuda, M.** Biodegradable polymer needle with various tip angles and consideration on insertion mechanism of mosquitos proboscis. *Sensors Actuators A*, 2008, **143**, 20–28.

10 **Izumi, H., Yajima, T., Aoyagi, S., Tagawa, N., Arai, Y., Hirata, M.,** and **Yorifuji, S.** Combined harpoon-like jagged microneedles imitating mosquitos proboscis and its insertion experiment with vibration. *IEEJ Trans. Electl Electronic Engng*, 2008, **3**, 425–431.

11 **Ramasubramanian, M. K.** Mechanics of a mosquito bite with applications to microneedle design. *Bioinspiration Biomimetics*, 2008, **3**, 046001.

12 **Quicke, D. L. J., Ralec, A. L.,** and **Vilhelmsen, L.** Ovipositor structure and function in the parasitic Hymenoptera with an exploration of new hypotheses. *Atti Acad. Naz. Ital. Entomol. Rc.*, 1999, **47**, 197–239.

13 **Vincent, J. F. V.** and **King, M. J.** The mechanism of drilling by wood wasp ovipositors. *Biomimetics*, 1995, **3**, 187–201.

14 **Vilhelmsen, L., Isidoro, N., Romani, R., Basibuyuk, H. H.,** and **Quicke, D. L.** Host location and oviposition in a basal group of parasitic wasps: the subgenual organ, ovipositor apparatus and associated structures in the Orussidae (Hymenoptera, Insecta). *Zoomorphology*, 2001, **121**, 63–84.

15 **Quicke, D. L. J.** Ovipositor mechanics of the braconine wasp genus Zaglyptogastra and the ichneumonid genus Pristomerus. *J. Nat. Hist.*, 1991, **25**, 971–977.

16 **Quicke, D. L. J.** and **Fitton, M. G.** Ovipositor steering mechanisms in parasitic wasps of the families Gasteruptiidae and Aulacidae (Hymenoptera). *Proc. R. Soc. Lond., B*, 1995, **261**, 99–103.

17 **Frasson, L., Parittotokkaporn, T., Schneider, A., Davies, B. L., Vincent, J. F. V., Huq, S. E., Degenaar, P.,** and **Baena, F. M. R.** Biologically inspired microtexturing: Investigation into the surface topography of next-generation neurosurgical probes. In Proceedings of the 30th Annual Conference of the IEEE Engineering in Medicine and Biology Society (*EMBS 2008*), Vancouver, British Columbia, Canada, 20–25 August 2008, pp. 5611–5614 (IEEE, New York).

18 **Parittotokkaporn, T., Frasson, L., Schneider, A., Huq, S. E., Davies, B. L., Degenaar, P., Biesenack, J.,** and **Baena, F. M. R.** Soft tissue traversal with zero net force: feasibility study of a biologically inspired design based on reciprocal motion. In Proceedings of the 2008 IEEE International Conference on *Robotics and biomimetics*, Bangkok, Thailand, 22–25 February 2008, pp. 80–85 (IEEE, New York).

19 **Varkey, L.** Quantifying the diffusivity of dye in the agar gel model of brain. Final 2006 RET Report, Research Experience for Teachers, National Science Foundation, Chicago Science Teachers Research Program, University of Illinois at Chicago, Chicago, Illinois, USA, 2006.

20 **Ritter, R. C., Quate, E. G., Gillies, G. T., Grady, M. S., Howard, M. A.,** and **Broaddus, W. C.** Measurement of friction on straight catheters in *in vitro* brain and phantom material. *IEEE Trans. Biomed. Engng*, 1998, **45**, 476–485.

21 **Fritsch, M. J.** and **Manwaring, K. H.** Neuroendoscopy: review of recent papers. *Crit. Rev. Neurosurg.*, 1998, **8**, 141–145.

22 **Frasson, L., Reina, S., Davies, B. L.,** and **Rodriguez y Baena, F. M.** Design optimization of a biologically inspired multi-part probe for soft tissue surgery. In Proceedings of the 11th International Congress of the IUPESM, *Medical physics and biomedical engineering*, Munich, Germany, 7–12 September 2009, pp. 307–310 (Springer).

23 **Webster, R. J., Kim, J. S., Cowan, N. J., Chirikjian, G. S.,** and **Okamura, A. M.** Nonholonomic modeling of needle steering. *Int. J. Robotics Res.*, 2006, **25**(5–6), 509–526.

24 **Minhas, D., Engh, J. A., Fenske, M. M.,** and **Riviere, C.** Modeling of needle steering via duty-cycled spinning. In Proceedings of the 29th Annual International Conference of the IEEE Engineering in Medicine and Biology Society (EMBS 2007), Lyon, France, 22–26 August 2007, pp. 2756–2759 (IEEE, New York).

25 **Kallem, V.** and **Cowan, N. J.** Image guidance of flexible tip-steerable needles. *IEEE Trans. Robotics*, 2009, **25**, 191–196.

26 **Glozman, D.** and **Shoham, M.** Image-guided robotic flexible needle steering. *IEEE Trans. Robotics*, 2007, **23**(3), 459–467.

27 **Murray, R. M., Li, Z.,** and **Shankar Sastry, S.** *A mathematical introduction to robotic manipulation*, 1994 (Taylor & Francis, London).

28 **Sethian, J. A.** Advances in fast marching and level set methods for propagating interfaces. In Proceedings of the International Conference on *Hyperbolic problems*, International Series of Numerical Mathematics, Vol. 130, Zürich, Switzerland, February 1998, 1999, pp. 855–864 (Birkhäuser, Basel).

29 **Petres, C., Pailhas, Y., Patron, P., Petillot, Y., Evans, J.,** and **Lane, D.** Path planning for autonomous underwater vehicles. *IEEE Trans. Robotics*, 2007, **23**(2), 331–341.

30 **Gousias, I. S., Rueckert, D., Heckemann, R. A., Dyet, L. E., Boardman, J. P., Edwards, A. D.,** and **Hammers, A.** Automatic segmentation of brain MRIs of 2-year-olds into 83 regions of interest. *NeuroImage*, 2008, **40**, 672–684.

31 BWH and 3D Slicer contributors, 3D Slicer, 2009 available from www.slicer.org.